Fuel 254 (2019) 115634

Contents lists available at ScienceDirect

Fuel

journal homepage: www.elsevier.com/locate/fuel

Full Length Article

End-gas autoignition characteristics of PREMIER combustion in a pilot fuel-ignited dual-fuel biogas engine

Alireza Valipour Berenjestanaki, Nobuyuki Kawahara, Kazuya Tsuboi, Eiji Tomita*

Department of Advanced Mechanics, Graduate School of Natural Science and Technology, Okayama University, Tsushima-Naka 3-1-1, Kita-Ku, Okayama 700-8530, Japan

ARTICLE INFO

Keywords:
Autoignition
Biogas
Dual-fuel engine
Pilot injection
Thermal efficiency

ABSTRACT

To improve the thermal efficiency of internal combustion engines at high loads, premixed mixture ignition in the end-gas region (PREMIER) combustion is proposed as a precursor to knocking. In the current work, a pilot fuel-ignited dual-fuel gas engine was operated at constant speed under different intake pressures (101, 150, and 200 kPa). A simulated biogas was served as the primary fuel and diesel as the pilot fuel. The maximum mean effective pressure and thermal efficiency were evident during PREMIER operation because of autoignition in the end-gas region. Similar to knocking combustion, PREMIER combustion features two stages but neither pressure oscillation nor a rapid pressure rise is observed. We here define a new parameter, the PREMIER intensity (PI), which reflects the strength of PREMIER combustion. As the injection timing was advanced and the pressure boosted, more cycles underwent end-gas autoignition; the associated heat release increased and, consequently, the PI value rose. When the pressure and temperature of a premixed fuel mixture rose as injection timing was advanced, end-gas autoignition commenced earlier. The end-gas autoignition delay became shorter as intake pressure was increased and injection timing advanced.

1. Introduction

Greenhouse gas (GHG) emissions are of serious environmental concern. Carbon dioxide (CO_2), methane (CH_4), nitrous oxide (N_2O), and fluorinated gases are all considered GHGs; they trap heat in the atmosphere. Carbon dioxide is typically produced by the burning of fossil fuels, and is thus of particular concern. Of the various GHGs, CO_2 contributes the most to climate change because of the enormous quantity that is emitted. Although CO_2 is also produced naturally, human activities greatly affect the amount in the atmosphere. Transportation, power generation, and other industrial purposes involving fossil fuel combustion are the principal human activities increasing the amount of atmospheric CO_2. Electricity demand continues to rise due to worldwide population growth and economic development. In terms of future energy demands, the depletion of petroleum resources is also of concern. Long-term use of petroleum derivatives as energy sources for transportation and power generation may not be feasible, given the dwindling global reserves, increasing costs, and environmental issues. The internal combustion engine situation is particularly critical; such engines are widely used in the automobile and electricity generation industries. Therefore, high-efficiency low-emission engines using more advanced combustion strategies, and new fuels that do not exploit conventional resources, are required. Extensive research is underway to identify alternative fuels and develop new combustion technologies.

One of the most suitable energy resources among alternative fuels for internal combustion engines is biomass gas, which is renewable, clean, and readily available [1,2]. Biomass is organic material from animals or plants. Burning of biomass releases stored energy. Biomass can be burned directly or converted into liquid and gaseous biofuels such as bioethanol, biodiesel, and biogas, which can then be used as fuels for transportation and electricity generation. Gaseous biofuels generated via CH_4 fermentation are termed digester gases. These gases are produced by anaerobic fermentation of organic matter or feedstocks, such as sewage sludge, agricultural and forest residues, manure, and garbage. Also, biomass can be converted into gaseous biofuel via thermochemical gasification. Gaseous fuels obtained in this manner are termed producer gases. Of the various gaseous fuels, biogas produced via CH_4 fermentation is regarded as a particularly promising alternative fuel for internal combustion engines. This biogas is composed principally of CH_4 (about 50–60%) and CO_2, and may be a useful fuel for power generation in rural areas. Biogas exhibits good anti-knocking properties because it includes CH_4. Global warming can be reduced by burning biogas, which can be used without any major modification of

* Corresponding author.
E-mail address: etomita@okayama-u.ac.jp (E. Tomita).

https://doi.org/10.1016/j.fuel.2019.115634
Received 20 February 2019; Received in revised form 30 April 2019; Accepted 11 June 2019
Available online 02 July 2019
0016-2361/ © 2019 Elsevier Ltd. All rights reserved.

Nomenclature

CH_4	Methane
CI	Compression ignition
CO	Carbon monoxide
CO_2	Carbon dioxide
$COV_{(IMEP)}$	Coefficient of variation of the indicated mean effective pressure
HC	Hydrocarbon
HCCI	Homogeneous charge compression ignition
IMEP	Indicated mean effective pressure
IVC	Intake valve close
KI	Knocking intensity
MFB	Mass fraction burned
N_2	Nitrogen
NO_x	Nitrogen oxide
PI	PREMIER intensity
PREMIER	Premixed mixture ignition in the end-gas region
Q_{ea}	Heat release due to end-gas autoignition
RCCI	Reactivity controlled compression ignition
ROHR	Rate of heat release
SI	Spark ignition
$\Delta\theta_{ea}$	Duration of heat release due to end-gas autoignition
θ_{ea}	End-gas autoignition timing
θ_{ign}	First ignition timing
θ_{inj}	Injection timing of pilot fuel
τ	Ignition delay of initial combustion
τ_{ea}	End-gas autoignition delay
°CA	Crank angle degree
°BTDC	Degree of crank angle before top dead center
°ATDC	Degree of crank angle after top dead center

spark ignition (SI) engines [3–5]. However, the combustion quality and thermal efficiency of engines fueled by biogas are reduced by the biogas CO_2. This gas reduces NO_x emission by decreasing the burning velocity, but increases hydrocarbon (HC) emission by reducing the combustion temperature. The high self-ignition temperature of biogas means that the fuel cannot be used alone in compression ignition (CI) engines. An ignition source is required; biogas is used in dual-fuel internal combustion engines. In a dual-fuel gas engine, gaseous fuel is introduced at the intake port, where it is mixed with air. As it is difficult to autoignite the mixture via compression only, liquid fuel is used to support ignition. The mixture is thus ignited by combustion of injected fuel. Gaseous dual-fuels have been extensively researched. Fundamental work on the use of such fuels was reviewed by Karim [6,7]. Walsh et al. extensively explored biogases for SI and CI engines [8]. The advantages and disadvantages of dual-fuel operation using different gaseous and pilot fuels [9–13], as well as fuel properties [14,15], fuel composition and quantities [16,17], exhaust gas recirculation (EGR) [13], injection timing [9,10,15,18,19], loads [9,17,20–22], speed [23,24], the equivalence ratio [25], and the compression ratio [12,20] have all been studied extensively. Overall, the dual-fuel strategy is the most promising way to exploit gaseous fuels. However, the amounts of such fuel that can thus be used are limited by knocking caused by rapid heat release [26–29].

Advanced combustion methods such as homogeneous charge compression ignition (HCCI) are more recent developments. These combustion methods were initially introduced to achieve significant reductions in NO_x and PM emissions while maintaining the thermal efficiency of CI engines. The HCCI combustion strategy features autoignition of an in-cylinder mixture [30–33]. Two drawbacks of HCCI combustion are that control of combustion timing is difficult, as is operation under high loads. HCCI engines emit more HCs and carbon monoxide (CO) than do diesel engines [31,34,35]. Although several improvements have been made, and modern HCCI engines are more thermally efficient, a risk of knocking caused by uncontrolled autoignition remains; therefore, a better combustion control strategy is required [36,37]. However, although the operation range of HCCI combustion has been extended, practical applications remain difficult. Therefore, combinations of HCCI combustion with either SI or diesel engines have been considered; ignition timing is controlled using a spark plug or via autoignition on fuel injection [38,39]. The operation of HCCI engines at high loads is compromised by knocking. Spark-assisted compression ignition (SACI) was introduced to extend the operation range of HCCI combustion while maintaining low emissions and high efficiency [40–45]. Spark timing controls autoignition and prevents accidental combustion. In [45], it was observed that the stability of gasoline HCCI combustion can be improved by spark assistance near the misfire limit. Nevertheless, combustion stability at higher loads remains problematic. Combustion control via diesel fuel injection is termed reactivity controlled compression ignition (RCCI) combustion [46–48]; this is a variant of HCCI combustion developed at the University of Wisconsin-Madison. The RCCI combustion concept was developed to control combustion via in-cylinder blending of two fuels with different reactivities via multiple injections. The RCCI method seeks to control combustion better, reduce NO_x and PM emissions, and improve fuel efficiency.

Although improved combustion efficiency is the goal of both HCCI and RCCI research, neither method is suitable for high-load operations. To improve the thermal efficiency of internal combustion engines at high loads, a different approach is required. The autoignition phenomenon that develops near the end-gas region often triggers knocking unless an appropriate combustion-controlling strategy is used. Knocking is the term used to describe unexpected/unwanted end-gas autoignition, and has been studied extensively [49–53]. Knocking is always unwanted because of its negative effects on engine components.

However, it was discovered that end-gas autoignition in the absence of pressure oscillations can improve engine operation at higher loads. This phenomenon has been termed premixed mixture ignition in the end-gas region (PREMIER) combustion [54]. We have studied such combustion using a dual-fuel gas engine operating under high loads. A second combustion that develops after the principal combustion of gaseous fuel and air is observed in the end-gas area in the absence of any pressure oscillation. Both the thermal efficiency and engine output are higher than those of normal combustion. Although several papers on PREMIER combustion have appeared, quantitative research data are not available. A parameter expressing the autoignition intensity is required when evaluating PREMIER combustion. Here, we evaluate the pressure, rate of heat release (ROHR), maximum pressure, ignition delay, engine performance, thermal efficiency, and end-gas autoignition characteristics of PREMIER combustion in great detail. The end-gas autoignition characteristics include autoignition timing, autoignition delay, the duration of heat release after autoignition, the mass fraction burned (MFB) before autoignition commences, and the amount of heat released. Moreover, we propose a new parameter that we term PREMIER intensity (PI); this allows quantification of PREMIER combustion.

2. PREMIER combustion

The PREMIER combustion strategy was developed to improve the performance and exhaust emission profile of internal combustion engines [9,54–62]. PREMIER combustion differs significantly from normal combustion and knocking combustion in its end-gas autoignition characteristics. After compression of gaseous fuel, some flame kernels are created via autoignition of the pilot fuel. Such autoignition triggers flame propagation within the gaseous fuel/air mixture. Combustion heat is released, and the in-cylinder pressure and temperature

increase further. From this point onward, the characteristics of unburned gas play an important role in determining the mode of combustion. The timing of autoignition in the end-gas region and the heat release characteristics determine whether knocking or PREMIER combustion ensues. PREMIER combustion differs from knocking combustion; particularly, the pressure oscillations characteristic of knocking are absent. A higher thermal efficiency and improved engine output are achieved when the engine operates in the PREMIER mode. Fig. 1 shows typical pressure histories and rates of heat release under normal, PREMIER, and knocking conditions [61]. When the injection timing is advanced from 3° before TDC (BTDC) to 6° BTDC, peaks in the pressure history and the ROHR are observed after a crank angle of 10° BTDC. These peaks indicate end-gas autoignition. High-frequency pressure oscillations are evident during knocking cycles; these are absent in the case of PREMIER combustion. During PREMIER combustion, the rises in pressure and ROHR are not as steep as those during knocking combustion.

Several experimental reports on dual-fuel engines, particularly those featuring PREMIER combustion, have appeared. Azimov et al. [54] published the first paper on PREMIER combustion. The cited authors experimented with a natural gas dual-fuel engine; they studied the effects of injection timing and EGR on the attainment and control of PREMIER combustion. Such combustion was achieved by advancing the injection timing. The OH radical emission levels were higher during knocking than PREMIER combustion cycles. In another study [58], the effects of syngas composition on dual-fuel engines operating in the PREMIER combustion mode were investigated. Under such conditions, the indicated mean effective pressure (IMEP) and thermal efficiency increased. When a split pilot fuel-injection strategy was applied to a dual-fuel natural gas engine, the PREMIER combustion operation range could be extended using an appropriately timed second injection [61]. Split fuel injection suppressed knocking combustion supported PREMIER combustion, promoted the transition from normal to PREMIER combustion, and further improved engine output and thermal efficiency. PREMIER combustion can also occur in SI engines [56]. Tomita et al. [56] visualized combustion using a compression-expansion machine (CEM); a high-speed camera was employed to confirm end-gas autoignition in the absence of pressure oscillation. Kawahara et al. [62] classified combustion states as normal, PREMIER, and knocking via in-cylinder pressure analysis and comparison of combustion flame images in terms of knocking intensity (KI). The auto-ignited flame area expanded faster during knocking than PREMIER combustion. The flame spread rates during both PREMIER and knocking combustion were measured to explore why PREMIER combustion is not accompanied by high-frequency pressure oscillations.

In terms of exhaust emissions, our previous studies [9,54,55,57–60] showed that CO and HC emissions decreased during PREMIER operation. These emissions are typically higher under dual-fuel operation but, in the PREMIER combustion mode, the levels decrease because of knock-free end-gas autoignition of the unburned mixture. Simultaneously, NO_x emissions increase because of the higher cylinder pressure and temperature attributable to autoignition in the end-gas region. Several strategies (such as EGR) have been introduced to decrease NO_x emissions, as have various treatment systems. However, NO_x reduction requires future study as PREMIER combustion strategies develop.

3. Experimental apparatus and data evaluation

We performed experiments using a single-cylinder, four-stroke, water-cooled, direct-injection, dual-fuel gas engine. A schematic diagram of the experimental setup is shown in Fig. 2. The engine had a bore and stroke of 96 and 108 mm, respectively, a displacement volume of 781 cm^3, and a compression ratio of 17:1. A diesel fuel injector with a three-hole nozzle (ϕ 0.1 mm) operating on a common rail system was used to spray the pilot fuel, which was pressurized employing a high-pressure oil pump. We sought to inject as little diesel fuel as possible. The crank angle (CA) signal was formed by the saw blades and a photodiode; the resolution was 0.5° when identifying the piston location. Simulated biogas served as the primary fuel and diesel as the pilot fuel. The biogas consisted of CH_4, CO_2, and N_2 at 58, 35, and 7% by volume, respectively. The gaseous fuel was introduced through an intake port; the gas flow rates were controlled using mass flow controllers. In-cylinder pressure was measured by a Kistler 6052C pressure transducer. A Kistler 5011 charge amplifier was used to amplify the in-cylinder pressure signal. All tests were conducted at an engine speed of 1000 rpm, and at three intake pressures (101, 150, or 200 kPa, established using a compressor). The pilot fuel was delivered at an injection pressure of 40 MPa at 0.8 mg/cycle. The overall equivalence ratio was set to 0.6 to achieve lean-burn combustion. Pilot fuel injection timing varied during the experiments. The engine details and experimental conditions are listed in Table 1.

As noted above, the first indicator of knocking is pressure oscillation. The pressure history and ROHR were averaged over 80 cycles for each dataset. To explore pressure oscillation, a band-pass filter (4–20 kHz) was applied to all pressure history data. The maximum instantaneous pressure difference between consecutive signals passing through the digital band-pass filter was defined as the KI. Any KI above a certain threshold (0.1 MPa) was defined as knocking. If even 1 of the 80 cycles exhibited a KI $>$ 0.1 MPa, we considered that knocking was present. In terms of PREMIER operation, we required that $>$ 50% of cycles should exhibit end-gas autoignition without knocking (i.e., KI $\leq$ 0.1 MPa) [50]. Any cycle exhibiting $<$ 50% end-gas autoignition was considered to correspond to normal combustion. Herein, we analyze the characteristics of PREMIER combustion in detail to confirm the presence of end-gas autoignition and a peak of heat release. The first ROHR peak corresponds to pilot fuel autoignition, the second to gaseous fuel-air combustion, and the third, which normally occurs after TDC, to end-gas autoignition.

Fig. 3 quantitatively explains PREMIER combustion and related parameters as well as ignition delay, τ. The ignition delay is defined the duration between injection timing to the first ignition timing. All parameters relevant to end-gas autoignition were obtained from the heat release rates. During PREMIER combustion, we determined θ_{ea} values from the times of inflection shown in the ROHR curves; this is also how we identified the timing of first ignition (θ_{ign}). The time interval between θ_{ign} and θ_{ea} is τ_{ea}. $\Delta\theta_{ea}$ begins at θ_{ea} and continues until end-gas heat release is complete. We also determined the amount of heat released due to end-gas autoignition (Q_{ea}). The PI value was determined using these parameters.

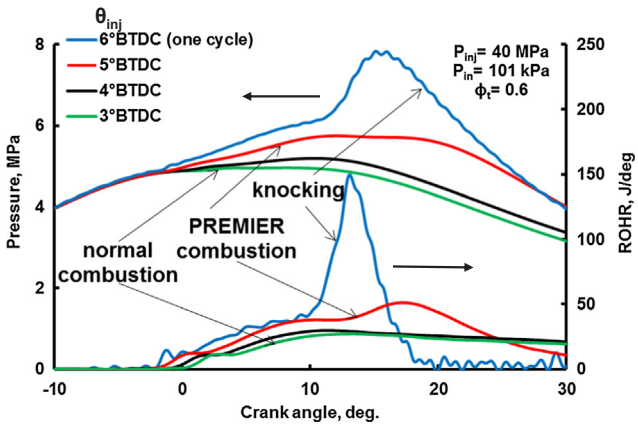

Fig. 1. Pressure history and rate of heat release during normal combustion, PREmixed Mixture Ignition in the End-gas Region (PREMIER) combustion, and the knocking cycles (primary fuel: natural gas) [61].

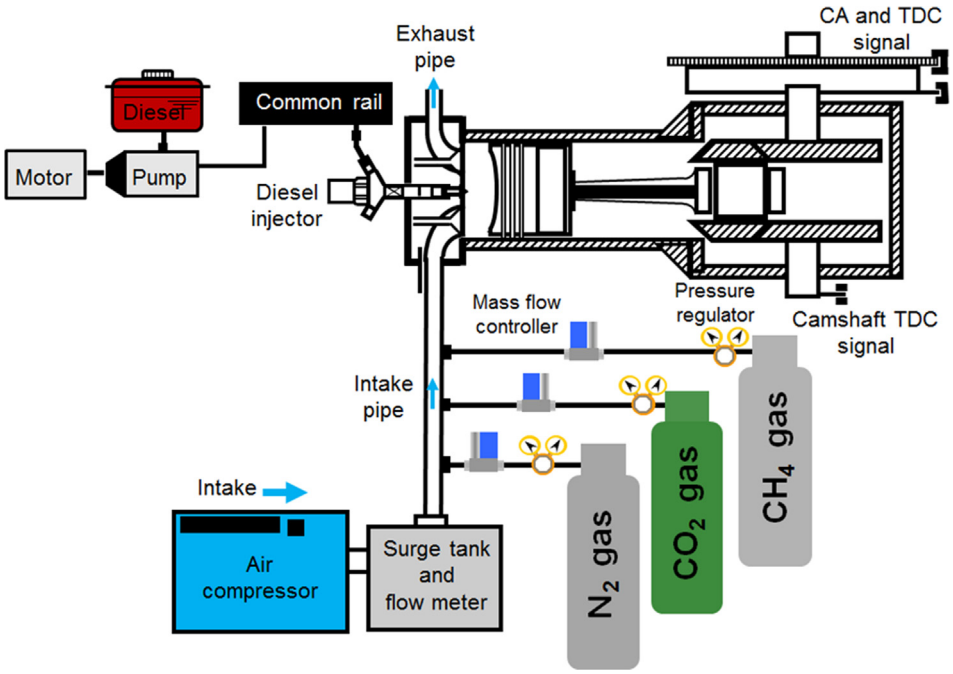

Fig. 2. Schematic diagram of the experimental setup.

Table 1
Test engine specification and experimental conditions.

Engine type	Four stroke, single cylinder
Bore × stroke	96 mm × 108 mm
Displacement volume	781 cm^3
Equivalence ratio, ϕ_t	0.6
Compression ratio	17:1
Combustion system	Pilot ignited dual fuel combustion
Intake pressure, P_{in}	101, 150, 200 kPa
Intake charge temperature	40 °C
Injection system	Common rail
Injection pressure	40 MPa
Injection quantity	0.8 mg/cycle
Nozzle hole × diameter	3 hole × ϕ 0.1 mm
Engine speed	1000 rpm
Injection timing of pilot fuel	15, 17, 20°BTDC at P_{in} = 101 kPa 10, 12, 14°BTDC at P_{in} = 150 kPa 8, 9, 10°BTDC at P_{in} = 200 kPa

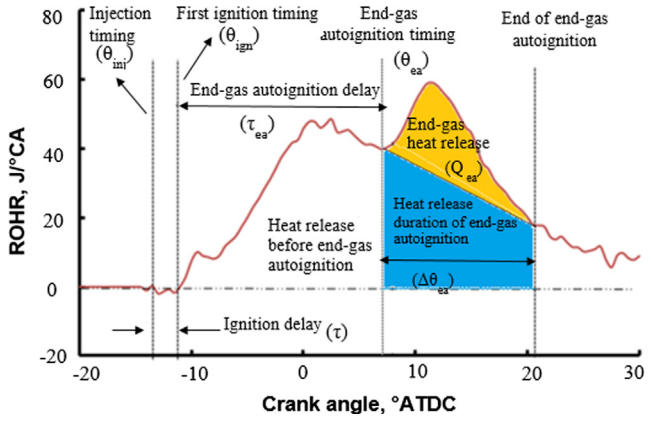

Fig. 3. Graphical representation of parameters describing PREMIER combustion.

4. Results and discussion

4.1. Cylinder pressure, rate of heat release, ignition delay, and maximum cylinder pressure

Fig. 4 shows the pressure history and ROHR at the three intake pressures of 101, 150, and 200 kPa. Both the maximum pressure and maximum ROHR increased when the pilot fuel injection timing, θ_{inj}, was advanced. Ignition delay (τ) is shown in Fig. 5. Higher intake pressures showed a shorter delay, attributable to the higher molar fraction of oxygen associated with the higher pressure. In Fig. 4(a), the first ROHR peak is that caused by pilot fuel autoignition can be observed clearly and it is 18.5 J/deg, however, when intake pressure is increased up to 150 kPa, the ROHR peak became smaller as shown in Fig. 4(b) and it is 16 J/deg. As shown in Fig. 4(c), at P_{in} = 200 kPa, the ROHR peak caused by pilot fuel autoignition was almost disappeared because the ignition delay is reduced by higher intake pressure. However, the ROHR peak of 11 J/deg was obtained from small inflation point of ROHR data for P_{in} = 200 kPa. In the dual-fuel combustion mode, ignition commences after pilot fuel injection near the end of the compression stroke, and the flame propagates through the gaseous fuel-air mixture. Advancing the injection timing increases the in-cylinder pressure because the combustion phase is also advanced. Advancing the injection timing from θ_{inj} = 15°BTDC to θ_{inj} = 17°BTDC for P_{in} = 101 kPa, from θ_{inj} = 12°BTDC to θ_{inj} = 14°BTDC for P_{in} = 150 kPa and from θ_{inj} = 8°BTDC to θ_{inj} = 10°BTDC for P_{in} = 200 kPa, increases in-cylinder pressure from 6 to 7.2 MPa, 8.8 to 10.5 MPa and 10.8 to 11.3 MPa, respectively. This allows autoignition of regions of unburned mixture before they can be consumed by propagating flames. The end-gas autoignition phenomenon can also be observed in the ROHR traces. Fig. 4(b) and (c) show that ROHR peaks were evident after TDC, attributable to autoignition of end-gas unburned mixture that had attained the required conditions after the injection timing was advanced. This was defined as PREMIER combustion. Under the conditions of Fig. 4(b) and (c), knocking occurred when the injection timing was further advanced, although the data are not shown. Similar findings were noted in previous work using different gaseous fuels (natural gas and hydrogen) [58]. Azimov et al. [58] reported that end-gas autoignition was affected by syngas composition.

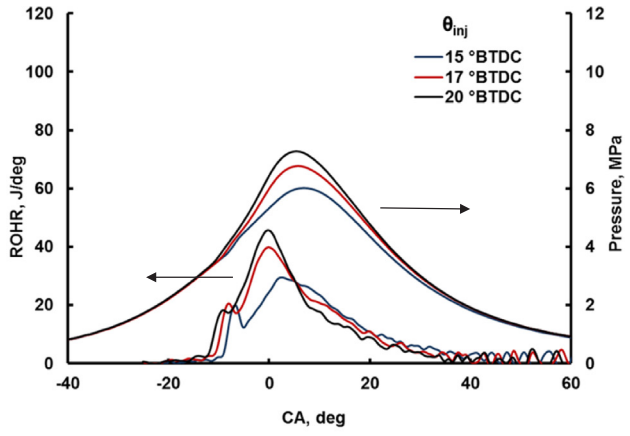

(a) P_{in} = 101 kPa

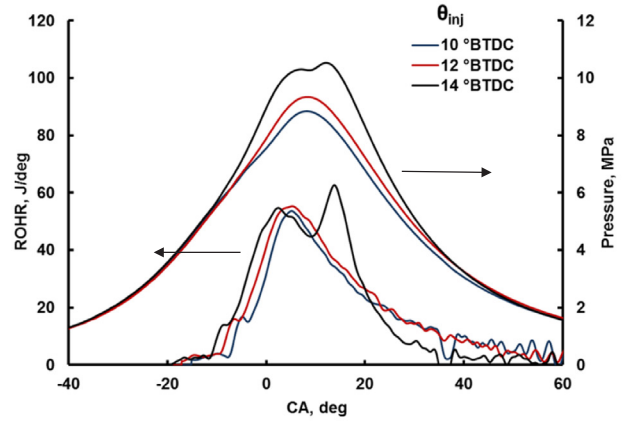

(b) P_{in} = 150 kPa

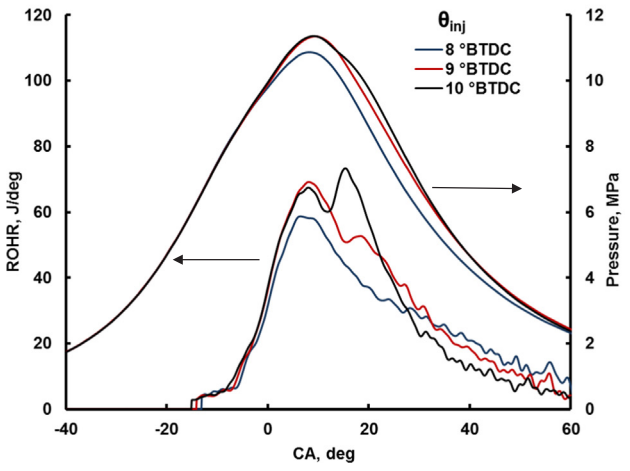

(c) P_{in} = 200 kPa

Fig. 4. Pressure history and rate of heat release for P_{in} = 101, 150 and 200 kPa.

The cited authors used seven different gaseous fuels, all of which exhibited PREMIER combustion.

The numbers of cycles exhibiting end-gas autoignition and KI are shown in Figs. 6 and 7 respectively. Fig. 6 shows that 77 cycles attained end-gas autoignition at θ_{inj} = 10° BTDC and P_{in} = 200 kPa, and that 60 cycles attained autoignition when θ_{inj} was 14° BTDC and P_{in} = 150 kPa. Both a higher intake pressure and advanced injection timing promoted PREMIER combustion. Fig. 7 shows that all cycles exhibiting end-gas autoignition were associated with KI values < 0.1 MPa. Given our

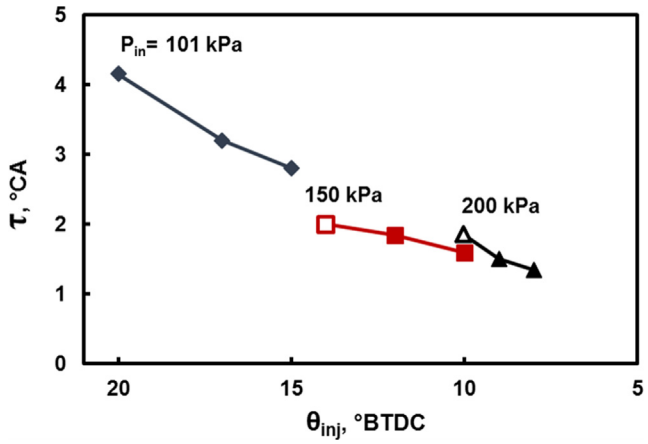

Fig. 5. Ignition delays of initial combustion.

definitions of PREMIER and knocking operations, these were considered to be knock-free cycles. Only the combinations of θ_{inj} = 10 and 14° BTDC, for P_{in} = 200 and 150 kPa, respectively, allowed PREMIER combustion; all other combinations were associated with normal combustion. At P_{in} = 101 kPa (only), injection timing advancement did not trigger end-gas autoignition. The maximum in-cylinder pressures are shown in Fig. 8 for all three intake pressures as injection timing changed. The maximum in-cylinder pressure was observed at θ_{inj} = 10° BTDC for P_{in} = 200 kPa, θ_{inj} = 14° BTDC for P_{in} = 150 kPa, and θ_{inj} = 20° BTDC for P_{in} = 101 kPa. A θ_{inj} = 10° BTDC for P_{in} = 200 kPa and a θ_{inj} = 14° BTDC for P_{in} = 150 kPa were defined as PREMIER conditions and are shown by open symbols. The higher maximum pressure of PREMIER combustion is attributable to end-gas autoignition of unburned mixture at a higher pressure and temperature.

4.2. Engine performance

Fig. 9(a), (b), and (c) show the IMEP, thermal efficiency, and coefficient of variation of the indicated mean effective pressure [$COV_{(IMEP)}$], respectively, as the pilot fuel injection timing changed. The performance data were determined from the pressure history. Fig. 9(a) shows that the highest IMEP values were observed during the PREMIER operation mode at θ_{inj} = 10° BTDC for P_{in} = 200 kPa and θ_{inj} = 14° BTDC for P_{in} = 150 kPa. The IMEP values increased as the injection timing advanced. The highest indicated thermal efficiency was observed at θ_{inj} = 10° BTDC for P_{in} = 200 kPa and θ_{inj} = 14° BTDC for P_{in} = 150 kPa; both occurred when PREMIER combustion was in play.

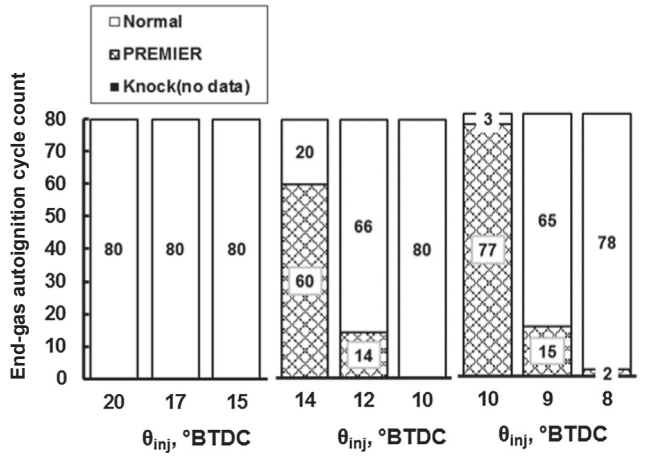

(a) P_{in}= 101 kPa (b) P_{in}= 150 kPa (c) P_{in}= 200 kPa

Fig. 6. Number of cycles featuring end-gas autoignition at all intake pressures.

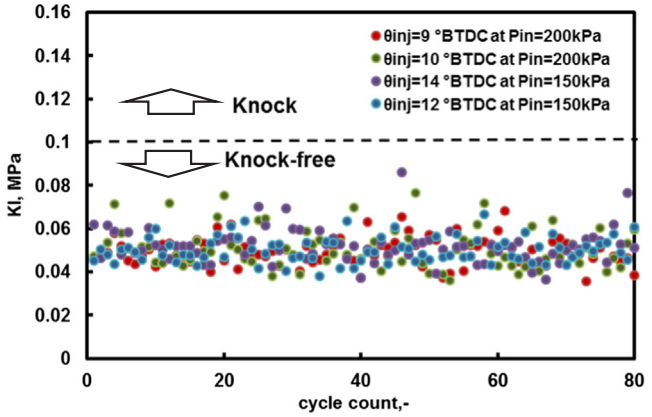

Fig. 7. Knocking intensity at P_{in} = 150 kPa and 200 kPa.

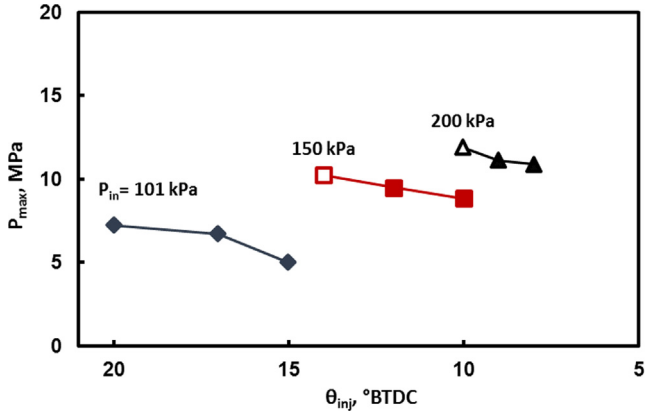

Fig. 8. Maximum cylinder pressure versus injection timing.

When the injection timing was advanced and PREMIER combustion achieved, the in-cylinder pressure increased because of the higher ROHR caused by end-gas autoignition of the unburned mixture. PREMIER combustion typically takes place during the expansion stroke; therefore, any pressure increase is followed by positive (volumetric) work and, consequently, enhanced IMEP and thermal efficiency. We earlier reported such improvements afforded by end-gas autoignition (in the PREMIER combustion mode) using different gaseous fuels [54,58–61]. Roy et al. [57] observed two-stage combustion as injection timing advanced; this afforded the highest IMEP and the best thermal efficiency. The stability of engine operation is indicated by the $COV_{(IMEP)}$; typically, better stability is associated with less output variation. The minimum $COV_{(IMEP)}$ was observed in the PREMIER operation mode. A lower $COV_{(IMEP)}$ reflects smoother engine operation. Roy et al. [57], Azimov et al. [58], and Aksu et al. [61] also reported stable combustion (< 4% variation) during PREMIER combustion of hydrogen and hydrogen-containing gaseous fuels, syngas, and natural gas in the dual-fuel mode. These facts are one of the features of PREMIER combustion. In consequence, improvement of engine performance under PREMIER combustion obtained from our previous experiments and this study shows the effectiveness of PREMIER combustion in dual-fuel combustion engines.

4.3. End-gas autoignition characteristics

4.3.1. End-gas autoignition timing and delay

The average θ_{ea} values of cycles exhibiting end-gas autoignition are shown in Fig. 10 with the standard errors. The θ_{ea} for PREMIER combustion was 8.24° after TDC (ATDC) for θ_{inj} = 14° BTDC at P_{in} = 150 kPa; and 11.21°ATDC for θ_{inj} = 10° BTDC at P_{in} = 200 kPa. Also, end-gas autoignition was observed when θ_{inj} = 9° BTDC and

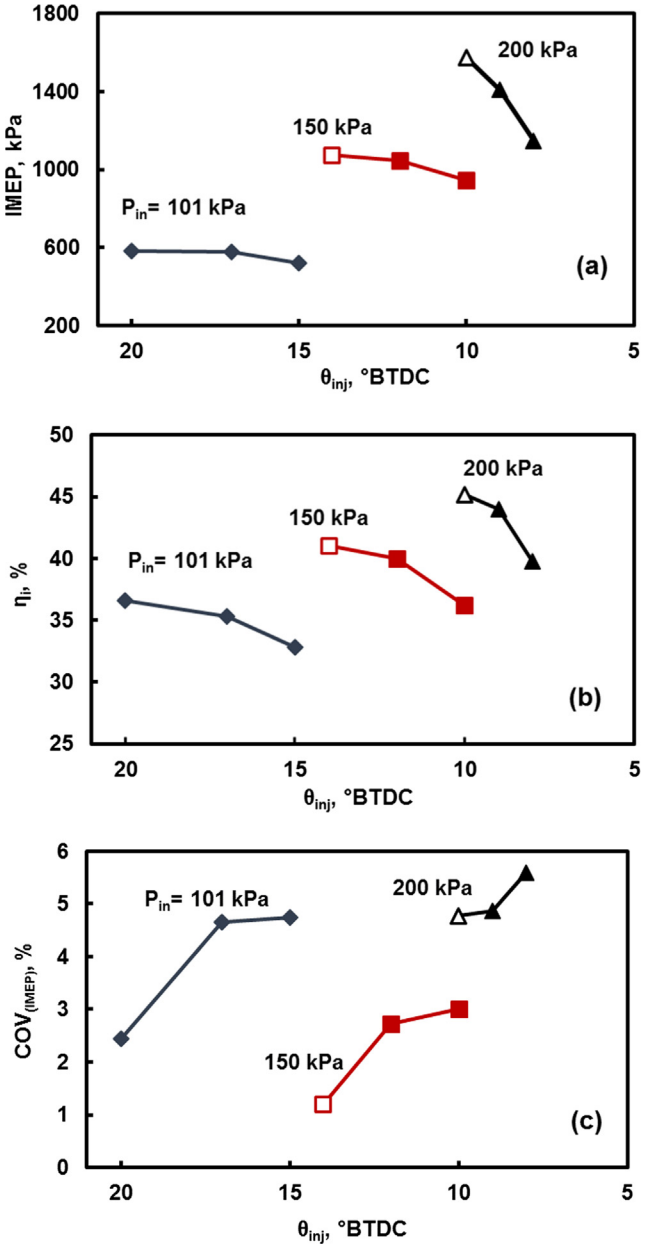

Fig. 9. Engine performance: (a) indicated mean effective pressure (IMEP); (b) indicated thermal efficiency; (c) coefficient of variation of the IMEP for P_{in} = 101, 150 and 200 kPa.

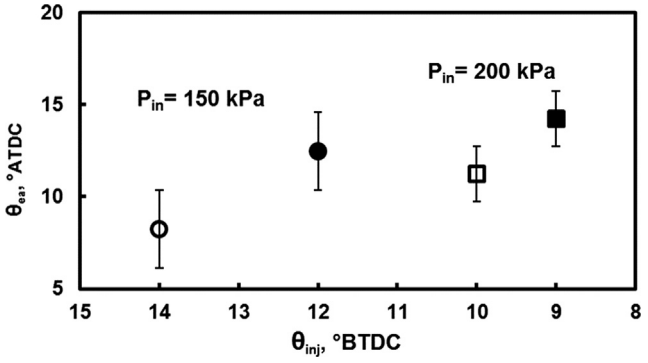

Fig. 10. Average end-gas autoignition timing, with standard error.

P_{in} = 200 kPa, and when θ_{inj} = 12° BTDC and P_{in} = 150 kPa, at 14.21° and 12.45° ATDC respectively. θ_{ea} was earlier when injection timing was advanced. The commencement of end-gas autoignition relies on the ROHR of the initial and principal combustion. Advancing injection timing results in higher combustion activity owing to the higher pressure and temperature of the unburned mixture during flame propagation; consequently, end-gas autoignition commences earlier. Fig. 11(a) and (b) illustrate unburned gas temperature from injection timing to end-gas autoignition timing at P_{in} = 150 kPa and P_{in} = 200 kPa, respectively. The process from intake valve close (IVC) to injection timing was determined from polytropic change in order to obtain temperature at injection timing. The process from injection timing to end-gas autoignition was determined from adiabatic change. As shown in Fig. 11(a), after injection timing, unburned gas temperature of θ_{inj} = 14° BTDC is slightly higher than that in θ_{inj} = 12° BTDC. Similarly, in Fig. 11(b), unburned gas temperature of θ_{inj} = 10° BTDC is slightly higher than that in θ_{inj} = 9° BTDC. A noticeable differences of unburned gas temperature between θ_{inj} = 14° BTDC and θ_{inj} = 12° BTDC at P_{in} = 150 kPa compared to θ_{inj} = 10° BTDC and θ_{inj} = 9° BTDC at P_{in} = 200 kPa is because of differences between their in-cylinder pressure as shown in Fig. 4(b) and (c). In consequence, higher temperature of the unburned mixture during flame propagation, causes earlier end-gas autoignition commencement.

The average τ_{ea} values of cycles exhibiting end-gas autoignition are shown in Fig. 12. The lowest τ_{ea} of 19.4° CA was observed for θ_{inj} = 10° BTDC at P_{in} = 200 kPa. As shown in Fig. 13, the lower τ_{ea} at P_{in} = 200 kPa compared to that at P_{in} = 150 kPa was attributable to the mass fraction burned (MFB) before end-gas autoignition commenced at θ_{ea}. When the intake pressure is higher, the unburned mixture is ignited more easily because of the shorter ignition delay. At P_{in} = 200 kPa, the MFB before autoignition in the end-gas region was smaller than that for P_{in} = 150 kPa. Less mixture was consumed during principal combustion (thus, during flame propagation). Autoignition develops in the end-gas region when the unburned mixture attains the required conditions. There are two possible outcomes after autoignition: flame development in the autoignition region or autoignition development. However, there is as yet no evidence that the phenomenon develops after end-gas autoignition commences.

4.3.2. The duration of heat release during end-gas autoignition

$\Delta\theta_{ea}$ is the time between the beginning and end of end-gas autoignition. The $\Delta\theta_{ea}$ values for cycles exhibiting end-gas autoignition are shown in Fig. 14. When the pressure and temperature of the unburned mixture region increase as a result of advancing the injection timing, the end-gas autoignition delay is reduced; however, this does not greatly affect the duration of heat release after end-gas autoignition. The effect of injection timing advancement was slightly greater at higher intake pressures. As shown in Fig. 13, a smaller proportion of the gaseous mixture was consumed by the propagating flame at P_{in} = 200 kPa than at P_{in} = 150 kPa. A larger mass in the end-gas region can also prolong the $\Delta\theta_{ea}$ if the temperature and pressure in that region at end-gas autoignition timing, θ_{ea}, do not rise significantly. This means that more unburned mixture remains for later autoignition when the autoignition conditions are ultimately attained. A larger mass in the end-gas region increases the KI during knocking cycles but the KI was almost unchanged during PREMIER cycles [62]. However, even when the end- gas mass was large, the KI of the PREMIER combustion can be lower than the threshold, thus preventing knocking when the duration of end-gas autoignition is prolonged. Also, there is a possibility of shorter duration of end-gas autoignition when strong knocking is occurred. In this case, duration of end-gas autoignition is shorter, however, high amount of heat is released from end-gas region followed by extremely high in-cylinder pressure. The peak after TDC (as a result of end-gasautoignition) in pressure history and ROHR is very steep compared to that in PREMIER combustion. In case of weak PREMIER combustion, neither sudden pressure rise nor high amount of heat release would not be occurred. If the end-gas autoignition conditions are satisfied later, $\Delta\theta_{ea}$ would be shorter because lower amount of heat released due to end-gas autoignition. When knocking occurs, PI value is expected to become large. In the present stage, discussion may be done qualitatively due to no knocking data. However, the criteria for PREMIER and knocking will be clarified in the future study.

4.3.3. Heat release after end-gas autoignition and PREMIER intensity

Quantification of PREMIER combustion was described above. A new parameter is needed to distinguish weak from strong end-gas autoignition. Therefore, we propose the PI, based on the end-gas autoignition data obtained from the heat release characteristics. The PI is defined as:

$$PI = \frac{100 * (Q_{ea}/Q_{total})}{\Delta\theta_{egai}} \quad (1)$$

where Q_{ea}, Q_{total}, and $\Delta\theta_{ea}$ are the amount of heat released due to end-gas autoignition, the total energy inputs of all fuels based on their lowest heating values, and the duration of heat release following end-gas autoignition, respectively. We exploit the relationship between the proportion of heat released due to end-gas autoignition and the duration of such release because this indicates the amount of heat released per unit time during such combustion. The yellow colored area in Fig. 3 (delimited by the straight dashed line) is defined as the region of end-gas autoignition heat release, obtained by examining the rates of heat release at the start and end of this time. The heat released via flame propagation during autoignition of the end-gas region is defined as the region below the straight line (blue colored area). The average Q_{ea} values of cycles exhibiting end-gas autoignition are shown in Fig. 15. As expected, the amount of heat released without knocking was maximal for θ_{inj} = 10° BTDC at P_{in} = 200 kPa. The number of cycles featuring end-gas autoignition was highest under these conditions; more heat

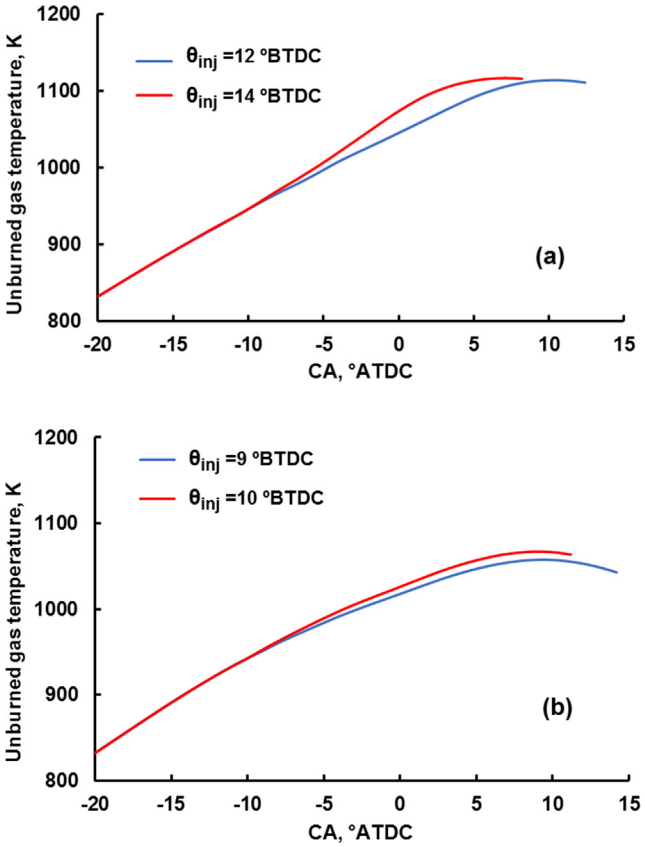

Fig. 11. Unburned gas temperature from injection timing of pilot fuel to end-gas autoignition timing at (a) P_{in} = 150 kPa and (b) P_{in} = 200 kPa.

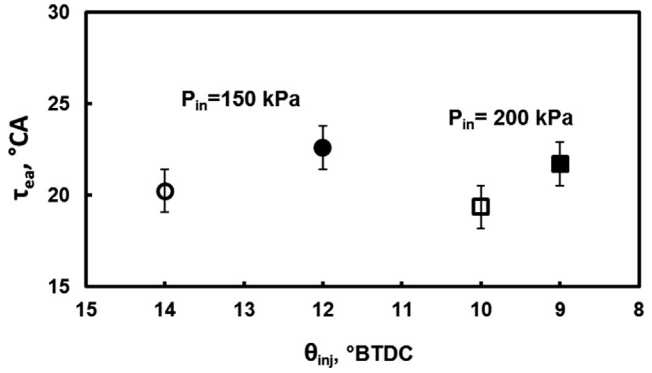

Fig. 12. Average end-gas autoignition delay, with standard error.

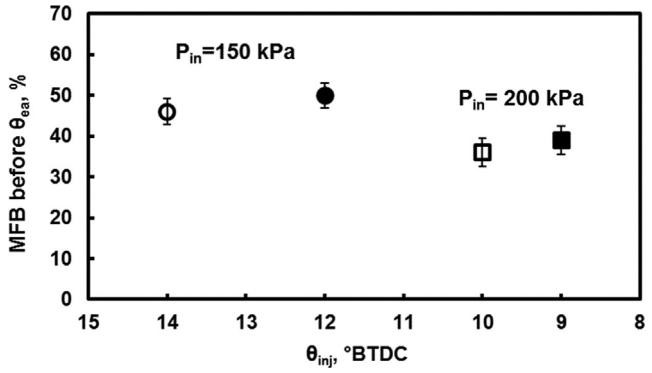

Fig. 13. Average mass fraction burned before commencement of end-gas autoignition for P_{in} = 150 kPa and 200 kPa, with standard error.

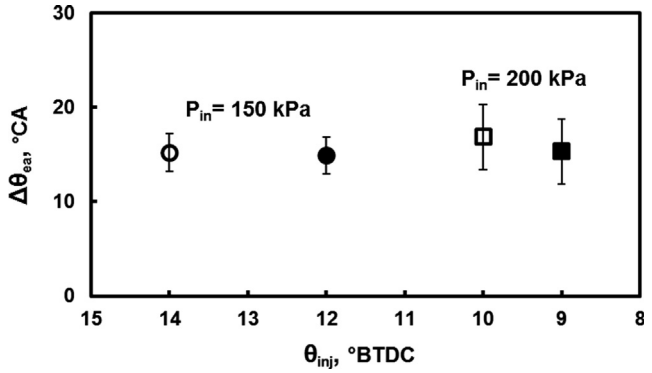

Fig. 14. Average heat release duration of end-gas autoignition for P_{in} = 150 kPa and 200 kPa, with standard error.

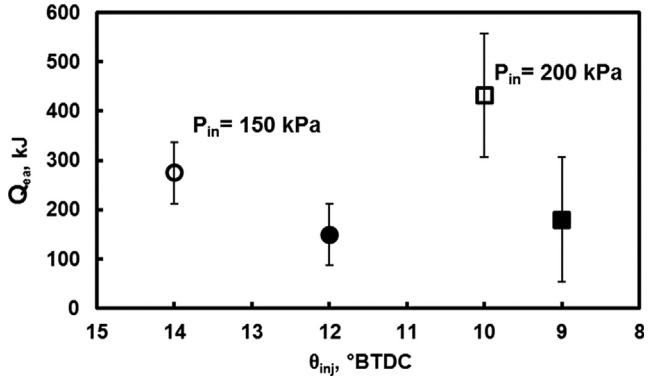

Fig. 15. Average heat release due to end-gas autoignition for P_{in} = 150 kPa and 200 kPa, with standard error.

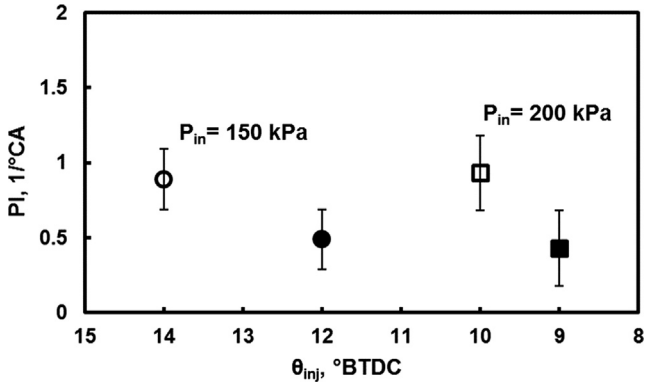

Fig. 16. Average PREMIER intensity for P_{in} = 150 kPa and 200 kPa, with standard error.

from the end-gas region was thus released. Consistent with Fig. 14, the longest $\Delta\theta_{ea}$ was observed at the same injection timing. The amount of heat released increased from 180 to 432 kJ when the injection timing was advanced from 9 to 10° BTDC at P_{in} = 200 kPa. For P_{in} = 150 kPa, the amount of heat released increased from 150 to 275 kJ when the injection timing was advanced from 12 to 14° BTDC. The number of cycles featuring end-gas autoignition increased from 15 to 77 at P_{in} = 200 kPa, and from 14 to 60 at P_{in} = 150 kPa, as shown in Fig. 6(b) and (c). The amount of heat released increased significantly as the number of end-gas autoignition cycles rose because of injection timing advancement. As shown in Fig. 16, experiments exhibiting higher numbers of end-gas autoignition cycles had higher PI values. The largest PI value was observed for θ_{inj} = 10° BTDC at P_{in} = 200 kPa, followed by θ_{inj} = 14° BTDC at P_{in} = 150 kPa.

The relationship between PI and the ratio of Q_{ea} to the total heat release, Q_{total}, and the relationship between PI and the heat release duration of end-gas autoignition (with standard errors), are shown in Fig. 17. Below, we clarify the relationships between these parameters. We found a strong association between the PI value and Q_{ea}/Q_{total}. The PI value increased in a near-linear manner with increasing Q_{ea}/Q_{total}. Cycles featuring more instances of end-gas autoignition exhibited higher Q_{ea}/Q_{total} values. Both Q_{ea}/Q_{total} and the PI value increased as injection timing was advanced: at θ_{inj} = 10° BTDC and P_{in} = 200 kPa, 77 cycles exhibited end-gas autoignition, compared to 60 cycles at θ_{inj} = 14° BTDC and P_{in} = 150 kPa [Fig. 6(b) and (c), respectively]. In Fig. 17, the Q_{ea}/Q_{total} at θ_{inj} = 10° BTDC and P_{in} = 200 kPa lies slightly above the linear trend line. The Q_{ea}/Q_{total} ratio rose during many cycles. Also, $\Delta\theta_{ea}$ increased at θ_{inj} = 10° BTDC and P_{in} = 200 kPa.

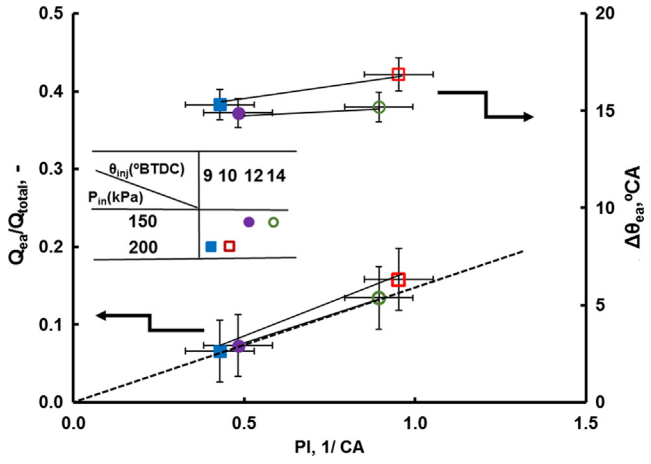

Fig. 17. The ratio of heat released due to end-gas autoignition to total heat release and PREMIER intensity (PI), and the heat release duration of end-gas autoignition by PI, with standard error.

According to Eq. (1), when $\Delta\theta_{ea}$ increases, the Q_{ea}/Q_{total} should rise to maintain the same PI value, but the PI value at $\theta_{inj} = 10^{\circ}$ BTDC and $P_{in} = 200$ kPa in fact increased. This is because much more heat was released in the end-gas region. As shown in Fig. 13, more unburned mixture remained in the end-gas region at $\theta_{inj} = 10^{\circ}$ BTDC and $P_{in} = 200$ kPa.

5. Conclusions

In this study, simulated biogas containing CH_4, CO_2, and N_2 was used as the primary fuel for a dual-fuel gas engine ignited using a pilot fuel (diesel). Experiments were performed at three intake pressures (101, 150, and 200 kPa), with the engine operating at a constant speed of 1000 rpm and with various pilot fuel injection times. Engine performance and the detailed end-gas autoignition characteristics were evaluated as the average of 80 cycles. We measured end-gas autoignition timing and delay, heat release duration, heat release amount, mass fraction burned before commencement of end-gas autoignition; and PI. We also quantified PREMIER combustion based on the end-gas heat release characteristics, as revealed by cycle-to-cycle analysis of each dataset. Furthermore, we defined a new parameter, PI. The following results were obtained:

1. The parameter PI was proposed and used to evaluate the characteristics of PREMIER combustion. The PI value increased as the heat released by end-gas autoignition increased, and as the duration of heat release was extended. However, the Q_{ea}/Q_{total} ratio affected the PI more so than did the $\Delta\theta_{ea}$.
2. When PREMIER combustion was achieved, the heat released by end-gas autoignition and the PI increased as the injection timing was advanced. Under such circumstances, the number of cycles featuring end-gas autoignition increased and more heat was released in the end-gas region.
3. The ROHR values of both the initial and main combustion affected the occurrence of end-gas autoignition. When the pressure and temperature of a premixed fuel mixture rose as injection timing was advanced, end-gas autoignition commenced earlier. The end-gas autoignition delay became shorter as intake pressure was increased and injection timing advanced, because of the lower MFB before end-gas autoignition commenced. Under these conditions, less mixture was consumed during principal combustion, and more was burned in the end-gas region.
4. Advancing the injection timing and increasing the intake pressure improved both the IMEP and thermal efficiency because end-gas autoignition then occurred. The higher the number of cycles featuring end-gas autoignition, the greater the thermal efficiency, because of the larger amount of positive work performed during the expansion stroke.

Acknowledgment

This work was supported by JSPS KAKENHI grant number 16H04601.

References

[1] Nathan SS, Mallikarjuna JM, Ramesh A. An experimental study of the biogas-diesel HCCI mode of engine operation. Energy Convers Manage 2010;51:1347–53.
[2] Henham A, Makkar MK. Combustion of simulated biogas in a dual-fuel diesel engine. Energy Convers Manage 1998;39:2001–9.
[3] Jawurek HH, Lane NW, Rallis CJ. Biogas/petrol dual fuelling of SI engine for rural third world use. Biomass 1987;13:87–103.
[4] Tewari P, Subrahmanyam J, Babu M, Experimental investigations on the performance characteristics of a producer gas fuelled spark ignition engine. SAE Technical Paper 2001-01-1189, 2001.
[5] Porpatham E, Ramesh A, Nagalingam A. Investigation on the effect of concentration of methane in biogas when used as a fuel for a spark ignition engine. Fuel 2007;87(8–9):1651–9.
[6] Karim GA. A review of combustion processes in the dual-fuel engine – the gas diesel engine. Prog Energy Combust Sci 1980;6:277–85.
[7] Karim GA, The dual-fuel engine of the compression ignition type – Prospects, problems and solutions – A review. SAE Technical Paper 831073, 1983, https://doi.org/10.4271/831073.
[8] Walsh JL, Ross CC, Smith MS, Harper SR. Utilization of biogas. Biomass 1989;20:277–90.
[9] Tomita E, Kawahara N, Kondo M, Sunada Y, Combustion and exhaust emissions characteristics of pilot-ignited engine fueled with digester gas; CIMAC congress, (2013), Shanghai, Paper No. 145.
[10] Barik D, Murugan S. Investigation on combustion performance and emission characteristics of a DI (direct injection) diesel engine fueled with biogas- diesel in dual fuel mode. Energy 2014;72:760–71.
[11] Feroskhan M, Ismail S. Investigation of the effects of biogas composition on the performance of a biogas-diesel dual fuel CI engine. Biofuels 2016;7:593–601.
[12] Bora BJ, Saha UK. Optimization of injection timing and compression ratio of a raw biogas powered dual fuel diesel engine. Appl Therm Eng 2016;92:111–21.
[13] Shan X, Qian Y, Zhu L, Lu X. Effects of EGR rate and hydrogen/carbon monoxide ratio on combustion and emission characteristics of biogas/diesel dual fuel combustion engine. Fuel 2016;181:1050–7.
[14] Cacua K, Amell A, Cadavid F. Effects of oxygen enriched air on the operation and performance of a diesel-biogas dual-fuel engine. Biomass Bioenergy 2012;45:159–67.
[15] Makareviciene V, Sendzikiene E, Pukalskas S, Rimkusb A, Vegneris R. Performance and emission characteristics of biogas used in diesel engine operation. Energy Convers Manage 2013;75:224–33.
[16] Barik D, Satapathy AK, Murugan S. Combustion analysis of the diesel-biogas dual fuel direct injection diesel engine– the gas diesel engine. Int J Ambient Energy 2015;38:259–66.
[17] Ambarita H. Performance and emission characteristics of a small diesel engine run in dual-fuel (diesel-biogas) mode. Case Stud Ther Eng 2017;10:179–91.
[18] Chandra R, Vijay VK, Subbarao PMV, Khura TK. Performance evaluation of a constant speed IC engine on CNG, methane enriched biogas and biogas. Appl Energy 2011;88:3969–77.
[19] Sahoo BB, Sahoo N, Saha UK. Effect of engine parameters and type of gaseous fuel on the performance of dual-fuel gas diesel engines—A critical review. Renew Sustain Energy Rev 2009;13:1151–84.
[20] Bora BJ, Saha UK, Chatterjee S, Veer V. Effect of compression ratio on performance, combustion and emission characteristics of a dual fuel diesel engine run on raw biogas. Energy Convers Manage 2014;87:1000–9.
[21] Ramesha DK, Bangari AS, Rathod CP, Chaitanya S. Combustion, performance and emissions characteristics of a biogas fuelled diesel engine with fish biodiesel as pilot fuel. Biofuels 2015;6:9–19.
[22] Uma R, Kandpal TC, Kishore VVN. Emission characteristics of an electricity generation system in diesel alone and dual fuel modes. Biomass Bioenergy 2004;27:195–203.
[23] Tippayawong N, Promwungkwa A, Rerkkriangkrai P. Long-term operation of a small biogas/diesel dual-fuel engine for on-farm electricity generation. Biosyst Eng 2007;98:26–32.
[24] Duc PM, Wattanavichien K. Study on biogas premixed charge diesel dual fuelled engine. Energy Convers Manage 2007;48:2286–308.
[25] Aklouche FZ, Loubar K, Bentebbiche A, Awad S, Tazerout M. Experimental investigation of the equivalence ratio influence on combustion, performance and exhaust emissions of a dual fuel diesel engine operating on synthetic biogas fuel. Energy Convers Manage 2017;152:291–9.
[26] Karim GA, An examination of some measures for improving the performance of gas fuelled diesel engines at light load. SAE Technical Paper 912366, 1991.
[27] Wang Zhongshu, Zhao Zhongxiang, Wang Dan, Tan Manzhi, Han Yongqiang, Liu Zhongchang, Dou Huili. Impact of pilot diesel ignition mode on combustion and emissions characteristics of a diesel/natural gas dual fuel heavy-duty engine. Fuel 2016;167:248–56. https://doi.org/10.1016/j.fuel.2015.11.077.
[28] Liu J, Zhang X, Wang T, Zhang J, Wang H. Experimental and numerical study of the pollution formation in a diesel/CNG dual-fuel engine. Fuel 2015;159:418–29.
[29] Tarabet L, Loubar K, Lounici MS, Khiari K, Belmrabet T, Tazerout M. Experimental investigation of DI diesel engine operating with eucalyptus biodiesel/natural gas under dual fuel mode. Fuel 2014;133:129–39.
[30] Dahl D, Denbrat I. HCCI/SCCI load limits and stoichiometric operation in a multicylinder naturally aspirated spark ignition engine operated on gasoline and E85. Int J Engine Res 2011;12:58–68.
[31] Singh AP, Agarwal AK. Combustion characteristics of diesel HCCI engine: an experimental investigation using external mixture formation technique. Appl Energy 2012;99:116–25.
[32] Jafarmadar S, Nemati P, Khodaie R. Evaluation of homogeneous charge compression ignition (HCCI) autoignition development through chemiluminescence imaging and proper orthogonal decomposition. Appl Energy 2018;210:288–302.
[33] Gharehghani A. Load limits of an HCCI engine fueled with natural gas, ethanol, and methanol. Fuel 2019;239:1001–14.
[34] Kim DS, Lee CS. Improved emission characteristics of HCCI engine by various premixed fuels and cooled EGR. Fuel 2006;85:695–704.
[35] Ganesh D, Nagarajan G. Homogeneous charge compression ignition (HCCI) combustion of diesel fuel with external mixture formation. Energy 2010;35:148–57.
[36] Andreae M, Cheng W, Kenney T, Yang J. On HCCI engine knock. SAE Technical Paper 2007-01-1858, 2007.
[37] Ma H, Xu H, Wang J, Tan C. Investigation on the self-stabilization feature of HCCI combustion. SAE Technical Paper 2014-01-2663, 2014.
[38] Manofsky Olesky LK, Middleton RJ, Lavoie GA, Wooldridge MS, Martz JB. On the

sensitivity of low temperature combustion to spark assist near flame limit conditions. Fuel 2015;158:11–22.
[39] Bendu H, Murugan S. Homogeneous charge compression ignition (HCCI) combustion: mixture preparation and control strategies in diesel engines. Renew Sustain Energy Rev 2014;38:732–46.
[40] Urushihara T, Yamaguchi K, Yoshizawa K, Itoh T, A study of a gasoline-fueled compression ignition engine – Expansion of HCCI operation range using SI combustion as a trigger of compression ignition, SAE Technical Paper 2005-01-0180, 2005.
[41] Xie H, Li L, Chen T, Yu W, Wang X, Zhao H. Study on spark assisted compression ignition (SACI) combustion with positive valve overlap at medium-high load. Appl Energy 2013;101:622–33.
[42] Lavoie G, Martz J, Wooldridge M, Assanis D. A multi-mode combustion diagram for spark assisted compression ignition. Combust Flame 2010;157:1106–10.
[43] Chiodi M, Kaechele A, Bargende M, Wichelhaus D, Poetsch Ch, Development of an innovative combustion process: spark-assisted compression ignition, SAE Technical Paper 2017-24-0147, 2017.
[44] Koch D, Berger V, Bittel A, Gschwandtner M, Wachtmeister G, Chiodi M, Kaechele A, Bargende M, Wichelhaus D, Investigation of an innovative combustion process for high-performance engines and its impact on emissions, SAE Technical Paper 2019-01-0039, 2019.
[45] Wang Zhi, Wang Jian-Xin, Shuai Shi-Jin, Tian Guo-Hong, An Xinliang, Ma Qing-Jun. Study of the effect of spark ignition on gasoline HCCI combustion. Proc Inst Mech Eng D J Automob Eng 2006;220(6):817–25. https://doi.org/10.1243/09544070JAUTO151.
[46] Splitter D, Wissink M, DelVescovo D, Reitz RD, RCCI engine operation towards 60% thermal efficiency. SAE Technical Paper 2013-01-0279, 2013.
[47] Li Y, Jia M, Chang Y, Xie M, Reitz RD. Towards a comprehensive understanding of the influence of fuel properties on the combustion characteristics of a RCCI (reactivity controlled compression ignition) engine. Energy 2016;99:69–82.
[48] Yang F, Yao C, Wang J, Ouyang M. Load expansion of a dieseline compression ignition engine with multi-mode combustion. Fuel 2016;171:5–17.
[49] Bates L, Bradley D, Gorbatenko I, Tomlin AS. Computation of methane/air ignition delay and excitation times, using comprehensive and reduced chemical mechanisms and their relevance in engine autoignition. Combust Flame 2017;185:105–16.
[50] Kawahara N, Tomita E, Sakata Y. Auto-ignited kernels during knocking combustion in a spark-ignition engine. Proc Combust Inst 2007;31:2999–3006.
[51] Bates L, Bradley D, Paczko G, Peters N. Engine hot spots: modes of auto-ignition and reaction propagation. Combust Flame 2016;166:80–5.
[52] Qi Y, Wang Z, Wang J, He X. Effects of thermodynamic conditions on the end gas combustion mode associated with engine knock. Combust Flame 2015;162:4119–28.
[53] Bradley D, Kalghatgi GT. Influence of autoignition delay time characteristics of different fuels on pressure waves and knock in reciprocating engines. Combust Flame 2009;156:2307–18.
[54] Azimov U, Tomita E, Kawahara N, Harada Y. Premixed mixture ignition in the end-gas region (PREMIER) combustion in a natural gas dual-fuel engine: operating range and exhaust emissions. Int J Engine Res 2011;12:484–97.
[55] Tomita E, Harada Y, Kawahara N, Sakane A, Effect of EGR on combustion and exhaust emissions in supercharged dual-fuel natural gas engine ignited with diesel fuel, SAE Technical Paper 2009-01-1832, 2009.
[56] Tomita E, Kawahara N, Zheng J. Visualization of auto-ignition of end gas region without knock in a spark-ignition natural gas engine. J KONES Powertrain Trans 2010;17:521–7.
[57] Roy MM, Tomita E, Kawahara N, Harada Y, Sakane A. Comparison of performance and emissions of a supercharged dual-fuel engine fueled by hydrogen and hydrogen-containing gaseous fuels. Int J Hydrogen Energy 2011;36:7339–52.
[58] Azimov U, Tomita E, Kawahara N, Harada Y. Effect of syngas composition on combustion and exhaust emission characteristics in a pilot-ignited dual-fuel engine operated in PREMIER combustion mode. Int J Hydrogen Energy 2011;36:11985–96.
[59] Azimov U, Tomita E, Kawahara N, Ignition, combustion and exhaust emission characteristics of micro-pilot ignited dual-fuel engine operated under PREMIER combustion mode, SAE Technical Paper; 2011-01-1764, 2011.
[60] Aksu C, Kawahara N, Tsuboi K, Nanba S, Tomita E, Kondo M, Effect of hydrogen concentration on engine performance, exhaust emissions and operation range of PREMIER combustion in a dual fuel gas engine using methane-hydrogen mixtures. SAE Technical Paper; 2015-01-1792, 2015.
[61] Aksu C, Kawahara N, Tsuboi K, Kondo M, Tomita E. Extension of PREMIER combustion operation range using split micro pilot fuel injection in a dual fuel natural gas compression ignition engine: a performance-based and visual investigation. Fuel 2016;185:243–53.
[62] Kawahara N, Kim Y, Wadahama H, Tsuboi K, Tomita E. Differences between PREMIER combustion in a natural gas spark-ignition engine and knocking with pressure oscillations. Proc Combust Inst 2019;37:4983–91.